Nonlinear optical response of a gold surface in the visible range: A study by two-color sum-frequency generation spectroscopy. I. Experimental determination

L. Dalstein, A. Revel, Christophe Humbert, Bertrand Busson

Nonlinear optical response of a gold surface in the visible range: A study by two-color sum-frequency generation spectroscopy. I. Experimental determination

L. Dalstein, A. Revel, C. Humbert, and B. Busson

Citation: The Journal of Chemical Physics **148**, 134701 (2018); doi: 10.1063/1.5021553
View online: https://doi.org/10.1063/1.5021553
View Table of Contents: http://aip.scitation.org/toc/jcp/148/13
Published by the American Institute of Physics

Nonlinear optical response of a gold surface in the visible range: A study by two-color sum-frequency generation spectroscopy. I. Experimental determination

L. Dalstein,[1,2] A. Revel,[1,3] C. Humbert,[1] and B. Busson[1]
[1]*Laboratoire de Chimie Physique, CNRS, Univ. Paris-Sud, Université Paris-Saclay, Bâtiment 201 P2, 91405 Orsay, France*
[2]*Department of Chemistry, School of Chemical Science and Engineering, KTH Royal Institute of Technology, SE-100 44 Stockholm, Sweden*
[3]*Grand Accélérateur National d'Ions Lourds (GANIL), CEA/DSM-CNRS/IN2P3, Blvd. Henri Becquerel, 14076 Caen, France*

(Received 5 January 2018; accepted 13 March 2018; published online 3 April 2018)

We experimentally determine the effective nonlinear second-order susceptibility of gold over the visible spectral range. To reach that goal, we probe by vibrational two-color sum-frequency generation spectroscopy the methyl stretching region of a dodecanethiol self-assembled monolayer adsorbed on a gold film. The sum-frequency generation spectra show a remarkable shape reversal when the visible probe wavelength is tuned from 435 to 705 nm. After correcting from Fresnel effects, the methyl stretching vibrations serve as an internal reference, allowing to extract the dispersion of the absolute phase and relative amplitude of the effective nonlinear optical response of gold in the visible range. *Published by AIP Publishing.* https://doi.org/10.1063/1.5021553

I. INTRODUCTION

Gold is used for a broad range of applications owing to its excellent chemical stability and high biocompatibility. This universality explains why gold has long been a choice substrate for nonlinear optical studies, both experimental[1] and theoretical.[2] However, its optical and plasmonic properties are complicated by strong and broad interband transitions below the plasma frequency, and fully understanding the nonlinear optical response of gold remains a challenge. Solving this complex case may therefore lay the foundations for new theoretical models and have broad applications to various systems involving metallic structures, from bulk to thin films and nanoparticles.

By and large, the majority of previous nonlinear optical studies on metallic surfaces have been conducted using second-harmonic generation (SHG) and focused on separating the various contributions to the experimental data by varying the polarizations[3] or angles of incidence[4] of the beams and the azimuthal orientations[5] of single crystals. By contrast, few experiments have investigated the nonlinear spectroscopic behavior of transition metals in the visible range,[5–9] owing to the additional experimental challenges: wavelength tunability of the laser source and broad spectral range detection. In addition, quantitative spectral analysis requires an absolute scale, which is difficult to achieve as visible and SHG wavelengths span the whole of the visible and part of the near-UV spectrum.

More recently, a number of infrared-visible sum-frequency generation (SFG) studies have also been conducted on gold, using it mostly as a substrate for investigating the molecular properties of adsorbed soft matter (mono)layers. In such experiments, only the infrared wavelength is tuned and the nonlinear signals from gold and molecular layers interfere in the SFG vibrational spectra.[10,11] Depending on the information sought, several strategies have been used to either remove the substrate contribution using broadband femtosecond setups[12,13] or obtain phase information from the interference pattern between gold and molecular contributions.[10,14] Alternatively, phase sensitive SFG experiments provide direct access to the absolute phase of the complex nonlinear response.[15]

The first report of a dispersion study of the nonlinear response from a gold surface measured by two-color (2C) SFG was conducted more than ten years ago.[16] Up to now, only few groups have implemented and routinely used a tunable visible arm in their SFG setup.[17–19] In principle, using a 2C-SFG setup, it should be possible to directly measure the absolute amplitude of the second-order nonlinear response of gold as a function of the tunable visible wavelength. Matranga *et al.*[8] have stressed the importance of conducting absolute measurements for the extraction of the nonlinear properties of metals. However, the intensity measured as the output of the 2C-SFG spectrometer encompasses several experimental factors that depend on the visible wavelength (laser beam propagation and overlap, detection efficiency). The dispersion of the SFG intensity in the visible range may therefore not be used straightforwardly and requires a proper intensity calibration of the setup. Some authors calibrate the intensities with an external reference sample (e.g., z-cut quartz), but this method requires to know the value of the nonlinear susceptibility of this reference sample as a function of the visible wavelength. For SHG experiments, they usually make use of Miller's rule in order to estimate this missing parameter.[8] However, this rule

remains approximate, especially toward the high energy end of the visible spectrum (which happens to correspond to the region where the efficiency of our detection system decreases) and has not been extensively tested for SFG experiments. In addition, such a calibrated 2C-SFG measurement on a gold surface would provide only the amplitude of the gold response, without any information on the phase.

To avoid these complexities, Ishibashi and Onishi[20] have adopted a new strategy to determine the dispersion of the SFG intensity of a gold substrate. Instead of using the gold contribution as a background for an adsorbed molecular layer, as is usually the case,[21] they calibrated the former with respect to the SFG response emitted by the latter used as an internal reference. This approach is justified by considering that the molecular nonlinear SFG susceptibility near a vibration mode is a complex Lorentzian function proportional to the anti-Stokes Raman cross section and infrared transition moment of that mode.[22] Therefore, it will not vary with the visible wavelength, provided that the Raman cross section does not become resonant nor pre-resonant (i.e., there is no molecular electronic transition in the visible and near-UV), and this is indeed the case for an alkanethiol. The advantages of this approach are that it avoids detection problems and characterization of the incoming beam intensities. In addition, as a consequence of the interference between resonant and non-resonant parts, the absolute phase information is also retained. Moreover, this additional parameter, specific to SFG and difference-frequency generation (DFG) among second-order nonlinear spectroscopies, helps us to further discriminate between the various parameter sets during data fitting[23] and imposes strong constraints on the theoretical modeling of the effective nonlinear susceptibility of gold, as the models should account for the experimental amplitude and phase instead of the amplitude alone.[8]

In this work, we analyze the two-color IR-visible SFG response of a polycrystalline gold layer functionalized by a dodecanethiol (DDT) monolayer. We show that molecular orientation and Fresnel factors must carefully be taken into account in order to analyze the dispersion of the molecular contribution toward SFG. Using this corrected molecular response to normalize the SFG signals of gold, we determine the effective gold nonlinear contribution by its amplitude line shape and absolute phase, as a function of the wavelength of the visible incoming beam tuned between 435 and 705 nm.

II. EXPERIMENTAL METHODS

A. Sum frequency (SFG) measurements

The SFG experimental setup has been described previously.[18,24] A picosecond Nd:YVO_4 (~10 ps pulse width, 62.5 MHz repetition rate, 1.064 μm wavelength) fundamental laser beam is amplified after temporal shaping in trains (125 pulses per 2 μs long train, repetition rate 25 Hz) by an acousto-optic modulator. The amplified output beam is then split into two in order to synchronously pump an infrared and a visible optical parametric oscillator (OPO), respectively. The IR-OPO is built around a $LiNbO_3$ crystal and pumped by the fundamental laser beam. The signal beam oscillates inside a cavity synchronized with the pulse repetition rate. In the present experiment, the output beam (idler) wavelength varies between 3.3 and 3.6 μm, with a bandwidth reduced to 2 cm^{-1} by a Fabry-Perot etalon located inside the cavity. The visible OPO is pumped by the third harmonics (355 nm) of the fundamental obtained after passing through a third harmonic generation stage composed of a β-barium borate (BBO) and a lithium triborate (LBO) crystal. The cavity is again synchronized with the repetition rate, and the oscillating signal, collected by a semi-transparent mirror, constitutes the visible laser output, tuned here between 435 nm and 705 nm. Both the IR and visible wavelengths are independently tunable. Both beams are mixed at the surface of the functionalized gold sample, with angles of incidence of 65° and 55° for the IR and visible beams, respectively. The three beams involved (SFG, visible, IR) are linearly p-polarized. The SFG signal is collected in reflection geometry and measured by a photomultiplier after spectral and spatial filtering through low pass filters and a double stage monochromator. A reference line collects in parallel the SFG photons produced in the bulk of a ZnS crystal, which are used to normalize the point-to-point laser fluctuations. SFG spectra are then recorded at the desired visible wavelength as a function of the IR wavelength.

B. Surface and SAM preparation

The substrate is a thin gold layer (250 nm) deposited on fused silica glass (Arrandee), cleaned first with acetone and ethanol, and then by butane flame annealing in order to improve the surface structure. Such a preparation scheme improves the homogeneity of the gold surface, leading to a surface organized mainly in (111) domains. It is well-known that such domains favor the growth of compact alkanethiol self-assembled monolayers (SAMs), inside which the interactions between neighboring alkane chains give rise to long range order with very few gauche defects. After immersion into a 10^{-3}M solution of dodecanethiol (DDT, Sigma Aldrich) in absolute ethanol (Sigma Aldrich) for 24 h, the DDT-functionalized sample is thoroughly rinsed in ethanol and dried under nitrogen flux before recording the SFG spectra in air.

III. THEORETICAL BACKGROUND AND DATA ANALYSIS

The SFG intensity radiated by a surface[25] in a ppp configuration is given by

$$I_p(\omega_{SFG} = \omega_{vis} + \omega_{IR}) = \frac{8\pi^3(\omega_{SFG})^2}{c^3\cos^2\theta_{SFG}}\left|\chi^{(2)}_{eff,ppp}\right|^2 I_p(\omega_{vis})I_p(\omega_{IR}), \tag{1a}$$

where θ_{SFG} is the angle of emission of the SFG beam in reflection, defined by the phase matching condition $\omega_{SFG}\sin\theta_{SFG} = \omega_{vis}\sin\theta_{vis} + \omega_{IR}\sin\theta_{IR}$, while $I_p(\omega)$ stand for the beam intensities at frequency ω and the refractive index of air is set to unity. The nonlinear second-order susceptibility tensor $\chi^{(2)}_{eff}$ encompasses all the contributions to the SFG intensity in our system: a surface term from the molecules ($\chi^{(2)}_{eff,mol}$) and one (mixing surface and bulk terms, $\chi^{(2)}_{eff,gold}$) from gold, which are both modeled by a complex number varying in a

general way with the visible (ω_{vis}) and infrared (ω_{IR}) frequencies. As explained in the Introduction, the molecular term solely depends on ω_{IR}, whereas the gold term varies with ω_{vis} and ω_{SFG}.

Interferences between gold and molecule contributions arise as a consequence of the summation of the $\chi^{(2)}{}_{eff}$ amplitudes, whereas only the intensities are experimentally measured

$$I_p(\omega_{SFG}) \propto \left|\chi^{(2)}_{eff,mol,ppp} + \chi^{(2)}_{eff,gold,ppp}\right|^2. \quad (1b)$$

As a consequence, a fitting stage of the experimental spectra is required to separate them. The SFG signals experimentally measured are proportional to the radiated intensity, taking into account an experimental, wavelength dependent, efficiency factor of the detection part of the setup.

We first focus on the molecular term, whose amplitude and phase must be determined over the probed infrared spectral range, as it serves as the internal reference for the effective gold contribution. According to symmetry rules applied to the in-plane isotropic surface, only components zzz, xxz, zxx, and xzx of the $\chi^{(2)}{}_{eff,mol}$ tensor do not cancel out in a ppp configuration, where (z) defines the surface normal (Fig. 1) and (x) defines the axis common to the surface and the plane of incidence (in other words, p⊥ and p∥,[3,26] respectively). This effective quantity includes projections along the coordinate axes and accounts for the actual local values of the electric fields as a consequence of transmission and reflection at the interfaces,

$$\chi^{(2)}_{eff,mol,ppp} = F_{zzz}\chi^{(2)}_{zzz} - F_{xxz}\chi^{(2)}_{xxz} + F_{zxx}\chi^{(2)}_{zxx} - F_{xzx}\chi^{(2)}_{xzx}, \quad (2a)$$

$$F_{zzz} = F_z(\omega_{SFG})F_z(\omega_{vis})F_z(\omega_{IR})\sin\theta_{SFG}\sin\theta_{vis}\sin\theta_{IR}, \quad (2b)$$

$$F_{xxz} = F_x(\omega_{SFG})F_x(\omega_{vis})F_z(\omega_{IR})\cos\theta_{SFG}\cos\theta_{vis}\sin\theta_{IR}, \quad (2c)$$

$$F_{zxx} = F_z(\omega_{SFG})F_x(\omega_{vis})F_x(\omega_{IR})\sin\theta_{SFG}\cos\theta_{vis}\cos\theta_{IR}, \quad (2d)$$

$$F_{xzx} = F_x(\omega_{SFG})F_z(\omega_{vis})F_x(\omega_{IR})\cos\theta_{SFG}\sin\theta_{vis}\cos\theta_{IR}. \quad (2e)$$

We note here that data analysis would have been much simpler if the ssp experimental configuration had been used.[25] However, in this case, the recorded SFG signals would have been too low, especially on the blue side of the spectrum, preventing an accurate determination of the gold response over the whole visible range. The definitions of Fresnel factors F_x and F_z are given in the supplementary material.[25] As for the complex refractive index of gold in the visible and the infrared, we have compared several sources (see the supplementary material for details) and chosen the tabulated data from a template-stripped gold film.[27] As a consequence of the very high refractive index of gold in the infrared, only the z-component of the incoming infrared electric field is not screened above the surface. In other words, F_{xzx} and F_{zxx} have very small values[28,29] (see the supplementary material for details), and xzx and zxx contributions may therefore be neglected in the following analysis.

In the probed infrared range, the terminal methyl moiety of DDT represents the dominant source of vibrationally resonant SFG in the molecular layer. The methylene signals cancel out for symmetry reasons in the absence of gauche defects, which is the case when the monolayer structure is close to a perfect SAM. The methyl groups produce three distinct vibrational features in the SFG spectra recorded in the CH stretching region, originating from the symmetric (ss) and antisymmetric (as) stretches, and a Fermi resonance (FR). In order to evaluate the relative weight of xxz and zzz for each resonance in $\chi^{(2)}{}_{eff,mol,ppp}$, we express these contributions as a function of the microscopic hyperpolarisability tensor β related to the CH_3 group. Under usual approximations (i.e., an isotropic surface, a unique molecular tilt angle with respect to the film normal, and visible wavelengths far from electronic resonances), it is well known that the CH_3 group, considered as a C_{3v} symmetric moiety, has three independent hyperpolarisability components: β_{ccc}, β_{aac}, and β_{aca},[30] where (c) is the symmetry axis of the methyl and (a) is an axis perpendicular to (c) in one of the three planes of symmetry.[31] They are related to the second-order susceptibility by the following laws:

$$\chi^{(2)}_{zzz}(ss) = N\beta_{ccc}\left[r_{a/c}\cos\theta_{CH_3} + (1 - r_{a/c})\cos^3\theta_{CH_3}\right], \quad (3)$$

$$\chi^{(2)}_{xxz}(ss) = \tfrac{N}{2}\beta_{ccc}\left[(1 + r_{a/c})\cos\theta_{CH_3} - (1 - r_{a/c})\cos^3\theta_{CH_3}\right], \quad (4)$$

$$\chi^{(2)}_{zzz}(as) = 2N\beta_{aca}\left[\cos\theta_{CH_3} - \cos^3\theta_{CH_3}\right] = -2\chi^{(2)}_{xxz}(as), \quad (5)$$

where θ_{CH_3} is the CH_3 tilt angle measured between molecular (c) and laboratory (z) axes, N is the surface density of CH_3 groups, and $r_{a/c}$ stands for β_{aac}/β_{ccc}. Owing to the origin of the

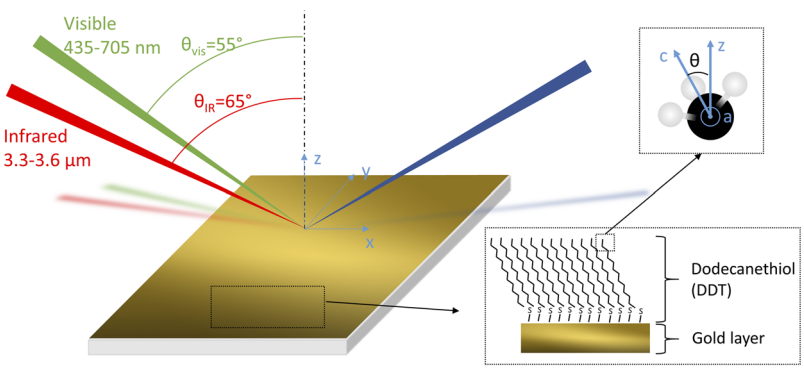

FIG. 1. Scheme of the experiment.

Fermi resonance, here we assume that its behavior is identical to that of the symmetric stretch.[32]

The overall molecular contribution follows

$$\chi^{(2)}_{\mathrm{eff,mol,ppp}} \approx F_{zzz}\chi^{(2)}_{zzz} - F_{xxz}\chi^{(2)}_{xxz} = \chi^{(2)}_{zzz}\left[F_{zzz} - F_{xxz}\frac{\chi^{(2)}_{xxz}}{\chi^{(2)}_{zzz}}\right], \tag{6}$$

with

$$\chi^{(2)}_{\mathrm{eff,mol,ppp}}(\mathrm{ss}) \approx \chi^{(2)}_{zzz}(\mathrm{ss})\,[F_{zzz} - F_{xxz}R] \equiv \chi^{(2)}_{zzz}(\mathrm{ss})F_{\mathrm{mol}}(\mathrm{ss,FR}),$$

where $R = \chi^{(2)}_{xxz}(\mathrm{ss})/\chi^{(2)}_{zzz}(\mathrm{ss})$ is a function of $r_{a/c}$ and θ_{CH_3}, and

$$\chi^{(2)}_{\mathrm{eff,mol,ppp}}(\mathrm{as}) \approx \chi^{(2)}_{zzz}(\mathrm{as})\left[F_{zzz} + \frac{F_{xxz}}{2}\right] \equiv \chi^{(2)}_{zzz}(\mathrm{as})F_{\mathrm{mol}}(\mathrm{as}).$$

Thus, for the total molecular contribution

$$\chi^{(2)}_{\mathrm{eff,mol,ppp}} \approx \left(\chi^{(2)}_{zzz}(\mathrm{ss}) + \chi^{(2)}_{zzz}(\mathrm{FR})\right)F_{\mathrm{mol}}(\mathrm{ss,FR}) + \chi^{(2)}_{zzz}(\mathrm{as})F_{\mathrm{mol}}(\mathrm{as}). \tag{7}$$

Finally, the molecular hyperpolarizabilities β and therefore intrinsic $\chi^{(2)}$(ss/FR/as) are described in the harmonic oscillator approximation[22] by a complex Lorentzian function, with a real numerator proportional to the infrared transition moment and anti-Stokes Raman amplitude, but independent of the visible wavelength.

Figures 2(a) and 2(b) show the evolution of the molecular F_{xxz} and F_{zzz} as a function of the visible wavelength. We immediately see that they do not share a common modulus and phase. As a consequence, the xxz and zzz contributions to the molecular $\chi^{(2)}$ cannot have the same phase during the fitting procedure, as is often done. This makes the fitting part even more complex, as has been shown in the past.[23] As for the (relative) phases between the three vibration modes, we may estimate them directly from Eq. (7), provided that quantity R (or $r_{a/c}$ and θ_{CH_3}) is known.

Using Eq. (7) and its counterparts for the other nonvanishing polarization contributions allows us to estimate the CH_3 tilt angle from experimental data, either by combining SFG measurements recorded for several polarization combinations[25] or several angles of incidence[33] or by comparing symmetric and antisymmetric stretches intensities.[32] In all cases, several parameters must be determined in order to complete the analysis, including the ratio $r_{a/c}$, the ratio $r_{A/S} = \beta_{aca}/\beta_{ccc}$, and the index of refraction of the molecular layer. Their values have a strong impact on the final results. We unfortunately find that there is no agreement on this point between various published articles, as the parameter values chosen in the literature depend on the nature of the molecule and on the method used to calculate them. For instance, several authors have used the bond additivity model,[31,34] while others prefer *ab initio*[35–37] or molecular dynamics methods[38] or link $r_{a/c}$ to Raman experimental depolarization ratios.[39] As a result, the values tabulated for $r_{a/c}$ in the literature range from 1.2 to 3.4.[25,32,40,41] Furthermore, for the $r_{A/S}$ ratio, existing controversy regarding the accuracy of the various methods[41] leads to an even wider range between 0.4 and 4.5.[34,36,40,41]

In the present study, we do not have sufficient information on the structure of our films to resolve the debate on these values nor to estimate the tilt angle for the CH_3 group. We therefore rely on a general analysis that takes into account broad distributions for the values assigned to $r_{a/c}$ and θ_{CH_3}.

First, we allow the ratio $r_{a/c}$ to vary between 1 and 4 and the CH_3 tilt angle to range from 10° to 60° (the most commonly encountered values lie around 50°) in order to evaluate the consequences of this choice on the molecular response of the monolayer on gold. Figure 3 shows the evolution of R in this range of parameters.

As R lies in the range of [0.89; 3.63], we use these values as limits to calculate (see the supplementary material for details) the modulus and phase of the molecular Fresnel contribution for the methyl symmetric stretching mode. In order to refine the analysis, we consider the two most popular values for $r_{a/c}$ (2.5[34] and 1.27[36]), leading to a R value lying in the interval [0.91; 2.37]. In order to visualize the results, the modulus and phase of the molecular symmetric stretch Fresnel contribution are shown in Figs. 2(c) and 2(d) for these two extremes and for two intermediate R values. It can be seen [Fig. 2(c)] that the phase does not heavily depend on R, i.e., on both $r_{a/c}$ and CH_3

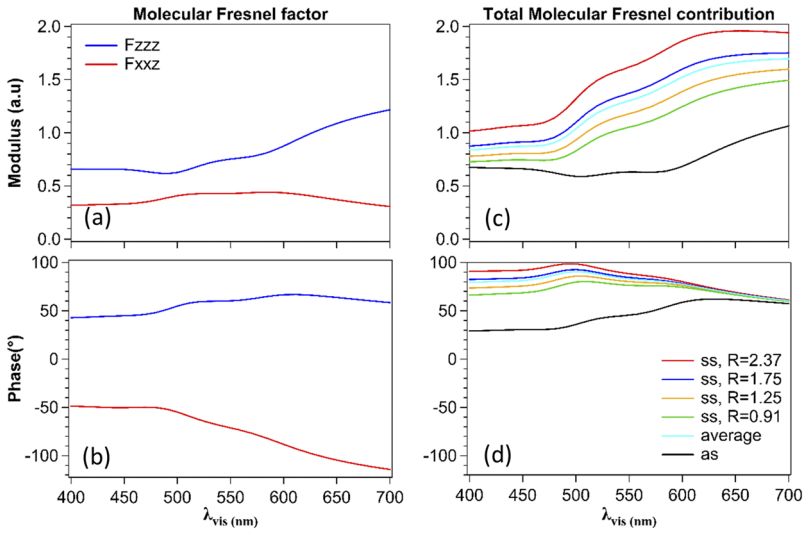

FIG. 2. Evolution of the modulus (a) and phase in degrees (b) of the molecular zzz and xxz Fresnel factors for a monolayer on gold and of the total molecular Fresnel contribution [(c) and (d)]. For the symmetric stretch, four values of $R = \chi^{(2)}_{xxz}(\mathrm{ss})/\chi^{(2)}_{zzz}(\mathrm{ss})$ are considered, the cyan curve is their average.

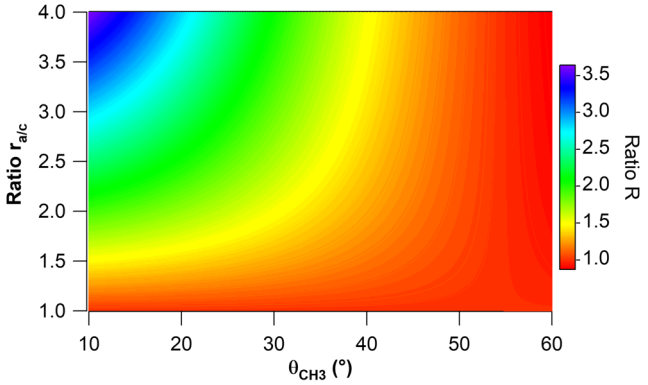

FIG. 3. Values calculated for ratio $R = \chi^{(2)}_{xxz}(ss)/\chi^{(2)}_{zzz}(ss)$ as a function of input parameters $r_{a/c} = \beta_{aac}/\beta_{ccc}$ (hyperpolarizabilty ratio) and θ_{CH_3} (CH_3 tilt angle measured between molecular c and laboratory z axes).

tilt angle, and that the modulus [Fig. 2(d)] keeps a constant line shape while its absolute amplitude remains in the same range of magnitudes. For these reasons, we conclude that the Fresnel contribution to the symmetric stretch does not heavily depend on the values chosen for R (i.e., $r_{a/c}$ and θ_{CH_3}). Therefore, for our analysis below, we use a mean value of $F_{mol}(ss, FR)$. We will thus be able to simulate an average molecular response and film structure.

When several SFG spectra are recorded with a tunable visible wavelength, as shown in Fig. 2(d), the phase shift between symmetric and antisymmetric stretches changes from 50° to almost zero from blue to red. This effect must be taken into account in the curve fitting, while caution is required when fitting SFG spectra with out-of-phase resonances,[23] as will be detailed below.

The phase shift tends toward zero at long visible wavelengths. As a consequence, broadband ppp SFG spectra recorded on alkanethiol monolayers on gold in usual conditions (visible wavelength close to 800 nm) may be fitted with all CH_3 resonances in phase. Furthermore, at such wavelengths, the refractive indices of gold for visible and SFG beams become almost imaginary, creating a 90° phase shift between F_x and F_z contributions. F_{xxz} and F_{zzz} thus present a 180° phase difference, which explains that the phase of F_{mol} remains constant whatever the weights of F_{xxz} and F_{zzz}. On the contrary, this is not valid for most picosecond setups, for which the visible beam wavelength is set at 532 nm, corresponding to a phase shift around 40°.

In a practical way, we fit the SFG spectra according to Eq. (8)

$$I(\omega_{SFG}) = \left| Ae^{i\phi} + \sum_{i=1,3} \frac{B_i}{\omega_{IR} - \omega_i + i\Gamma_i} \right|^2 \propto \left| \chi^{(2)}_{eff,ppp} \right|^2, \quad (8)$$

where ω_i and Γ_i stand for the resonance frequencies damping constants of the vibration modes, respectively. The summation runs over the three CH_3 modes, represented by Lorentzian functions. The experimental profiles result from the convolution between the intrinsic Lorentzian profiles and a Gaussian distribution due to both experimental resolution and inhomogeneous broadening,[42] resulting in a so-called Voigt profile. The signal-to-noise ratio of our experiments makes Voigt and Lorentzian profiles undistinguishable.[43] The nonlinear gold contribution (often called nonresonant, NR) is expressed in terms of modulus A and phase ϕ, which are both dependent on the visible and SFG wavelengths. The three vibrational amplitudes B_i are complex numbers and B_{as} is out of phase with B_{ss} and B_{FR}. We impose a null phase to the symmetric stretch contribution B_{ss} during the fits, in order to set the origin of the phases. Once the molecular effective nonlinear susceptibility is extracted from the experimental data by curve fitting, the contributions from the three vibrations are then separated and appropriately weighted in amplitude and in phase.

In the final step, we may therefore use any vibration mode, for example, the symmetric stretch, as the internal reference. By rewriting the full ppp effective second-order susceptibility, and retaining only the ss contribution, we obtain

$$\chi^{(2)}_{eff,ppp} = F_{mol}(ss)\chi^{(2)}_{zzz}(ss) + F_{gold}\chi^{(2)}_{gold}. \quad (9)$$

From the theoretical analysis, we know that the Lorentzian amplitude of the zzz component of $\chi^{(2)}$ has a vanishing phase. In order to link it to experimental data fitting, we write

$$\chi^{(2)}_{eff,ppp}(ss)e^{-i\arg(F_{mol}(ss))} = \chi^{(2)}_{zzz}(ss)\,|F_{mol}(ss)| + F_{gold}\chi^{(2)}_{gold}e^{-i\arg(F_{mol}(ss))}. \quad (10)$$

Thus, the amplitude of the effective nonlinear susceptibility of gold is obtained as

$$\left|F_{gold}\chi^{(2)}_{gold}\right| = (A/B_{ss})\left|\chi^{(2)}_{zzz}(ss)\right|\left|F_{mol}(ss)\right|, \quad (11)$$

where $\left|\chi^{(2)}_{zzz}(ss)\right|$ is an unknown and dispersionless constant, and its absolute phase is determined by

$$\arg\left(F_{gold}\chi^{(2)}_{gold}\right) = \phi + \arg(F_{mol}(ss)). \quad (12)$$

In the following, we present the experimental SFG results and analyze them as detailed above in order to extract the quantities defined in Eqs. (11) and (12), and their evolution over the visible range.

IV. RESULTS

Figure 4 displays the SFG spectra recorded as a function of the IR wavenumber for 15 visible wavelengths. All the spectra display the expected three CH_3 vibration modes from the terminal methyl group of the adsorbed DDT molecules, identified as the symmetric stretch (ss, 2875.2 cm^{-1}), antisymmetric stretch (as, 2962.0 cm^{-1}), and Fermi resonance (FR, 2935.5 cm^{-1}). No clear signal arises from the CH_2 groups of the alkane chain, indicating a long range order inside the DDT monolayer, with few gauche defects,[36] which means that the thiol molecules adopt indeed a SAM structure on the surface. The vibrational features interfere with the gold contribution, which appears as a constant baseline on the spectra. The rather drastic evolution in the vibrational line shape from blue to red indicates a change in both the phase shift and the amplitude ratio between the monolayer and gold contributions while scanning the visible range. Recording the full spectra allows determining these two quantities after curve fitting.

The sets of fitting parameters, one for each spectrum, must remain coherent over the whole visible range (in particular, the resonance frequencies and widths must be identical for all

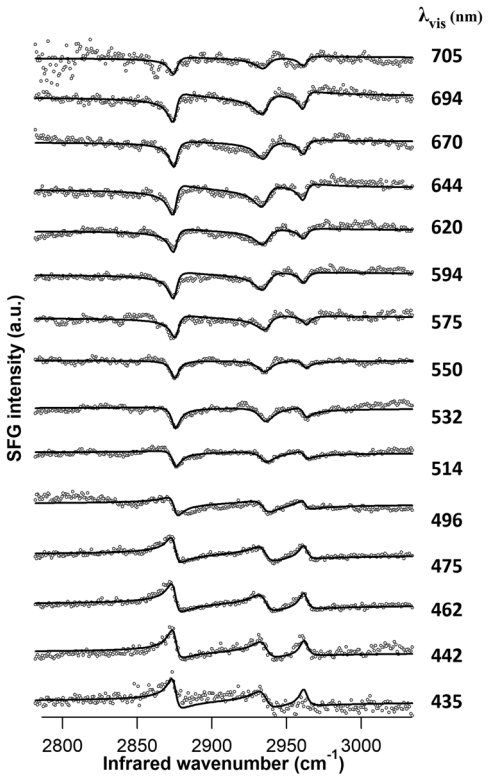

FIG. 4. SFG spectra of the system Au/DDT. The SFG intensity is recorded as a function of the IR wavenumber for the 15 visible wavelengths (λ_{vis}) indicated on the graph then corrected for incoming visible intensity, photomultiplier efficiency, and $(\omega_{SFG})^2$. The spectra are offset for clarity, each spectrum is displayed full scale in order to easily visualize the resonant features, along with model fits using Eq. (8).

spectra). As detailed in the supplementary material, the fits have been performed in several stages, during which some parameters were kept constant as they were determined during previous steps. We have also relied on the phase values reported by several other studies at 532 nm and cross-checked these by either comparison to DFG[14] or phase-sensitive measurements,[15] which were all around 90° at this wavelength. In the final step, the ratios of the amplitudes and the phase shifts between the three modes were kept fixed to a constant value modulated by F_{mol} for all spectra, as displayed in Figs. 2(c) and 2(d). In this way, it becomes possible to compare the non-resonant modulus and phase to that of any of the three vibration modes. We chose the symmetric stretch as in Eqs. (9)–(12). The corresponding fitting curves appear in Fig. 4, whilst the main fit parameters (A, B_{ss}, and ϕ) are shown in Fig. 5 together with the original values of Ishibashi and Onishi[20] For completeness, a list of all fit parameters may also be found in the supplementary material and show good agreement with those previously reported.

As explained in the previous part, Fig. 5 displays the amplitudes and phases of the molecular and gold contributions to the spectra as experimentally measured. In order to determine the true amplitude and phase of the gold contribution, we use Eqs. (11) and (12) to get rid of the influence of factor F_{mol}. The value deduced for $F_{gold}\chi^{(2)}_{gold}$ is displayed in Fig. 6 in terms of modulus and phase. The amplitude consists of a slowly growing background (from blue to red), on top of which a broad maximum raises it by a factor of

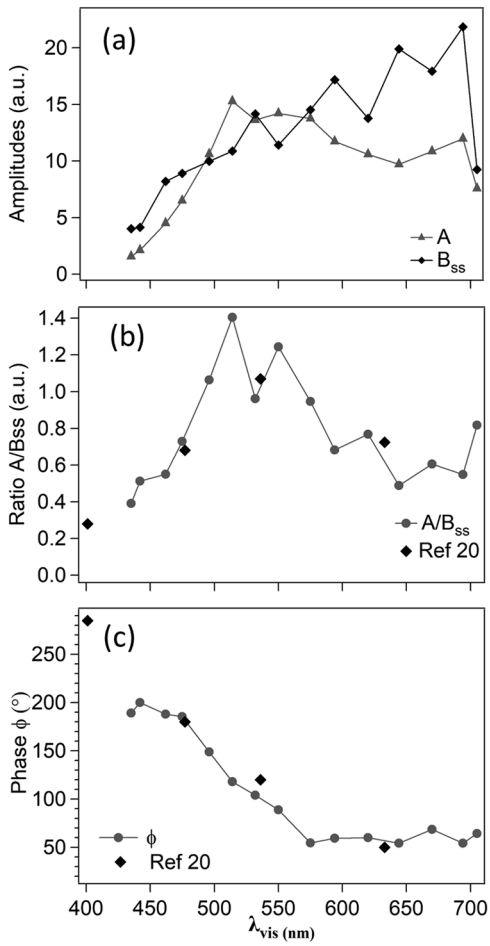

FIG. 5. Fit parameters deduced from Fig. 4: the amplitudes of the non-resonant A and symmetric stretch B_{ss} (a), the ratio of A/B_{ss} (b), and the non-resonant phase Φ (c). Experimental data from Ref. 20 are also shown in (b) and (c) for comparison.

approximately three. There are several possible origins for this line shape: (i) a resonant source through the excitation

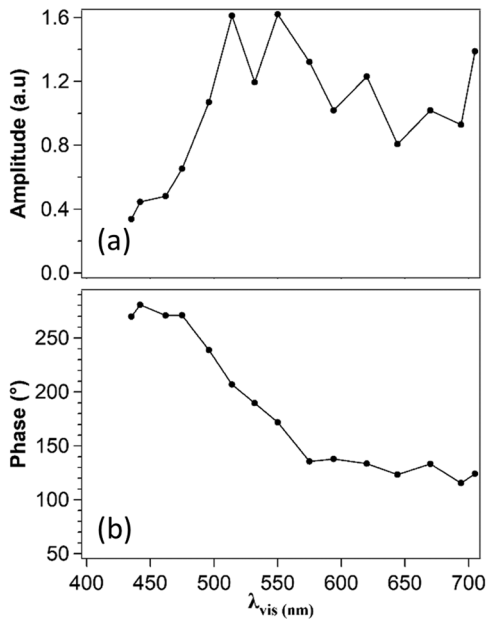

FIG. 6. Amplitude (a) and absolute phase (b) of the effective nonlinear response of gold in the visible range.

of a surface state, (ii) the dispersion of Fresnel factors for the gold substrate, and (iii) the intrinsic bulk and surface nonlinear response of gold. Yet, it is also conceivable that these may all work together. As a first approximation, the observed behavior may be qualitatively described by the sum of a free electron term, which should increase in magnitude toward the red end of the spectrum, and a bound electron term, resonant with interband transitions. These start around 620 nm[44] and extend toward the blue region, meaning that, in all our experiments, at least one of the beams excites them. Such a crude explanation favors points (ii) and (iii), even if it does not directly account for the decrease in amplitude toward the blue end of the spectrum. On the contrary, Ishibashi and Onishi[20] have shown the consistency of their data with the excitation of a phenomenological surface state, i.e., point (i), even if Fresnel effects were not included. This shows that a dedicated analysis of the nonlinear activity of gold in the visible range is required in order to settle this debate.

As for the phase, it may be treated as an almost complete sign reversal over the visible range. This phase parameter becomes very discriminating when comparing experimental data to the models used to describe the nonlinear response of gold. It is in fact more informative to experimentally measure both the absolute phase and the amplitude line shape, compared to the absolute modulus alone.

V. SUMMARY AND CONCLUSIONS

We have shown that it is possible to experimentally measure the effective nonlinear susceptibility of gold in a SFG experiment as a function of several different wavelengths over the visible range. By using an adsorbed self-assembled monolayer as an internal reference, we have removed all complexities related to incoming beam intensities and detection efficiency. In addition, we have gained additional information through the phase, due to the interference between molecular and gold contributions. In order to extract the appropriate quantities from experiment, rigorous care must be taken when considering the molecular properties and Fresnel factors, and data fits must remain consistent between all spectra.

The results in Fig. 6 constitute the main experimental result of this paper and the basis of the analysis of the sources of nonlinearities inside gold which may give rise to these quantities. In order to analyze and interpret the data of Fig. 6 further, a global approach is required which integrates the three causes outlined above, with a careful estimation of the respective weightings of the various contributions from the components of the surface and bulk gold nonlinear activity, scaled by their respective Fresnel activities. In Paper II,[45] we present a detailed theoretical analysis of the origin of the measured nonlinear effective activity from the gold surface and bulk, in order to compare it to the results presented here.

SUPPLEMENTARY MATERIAL

See supplementary material for additional data and methods about the choice of the bibliographical sources for the refractive index of gold, the dispersion of molecular Fresnel factors over the visible range, details and parameters for curve fitting and data scaling, and comparison of our results with the existing literature.

[1] N. Bloembergen, R. K. Chang, and C. H. Lee, Phys. Rev. Lett. **16**, 986 (1966).
[2] S. S. Jha and C. S. Warke, Phys. Rev. **153**, 751 (1967).
[3] D. Krause, C. W. Teplin, and C. T. Rogers, J. Appl. Phys. **96**, 3626 (2004).
[4] K. A. O'Donnell and R. C. Torre, New J. Phys. **7**, 154 (2005).
[5] E. K. L. Wong and G. L. Richmond, J. Chem. Phys. **99**, 5500 (1993).
[6] G. Petrocelli, S. Martellucci, and R. Francini, Appl. Phys. A: Mater. Sci. Process. **56**, 263 (1993).
[7] H. Tanaka, H. Wakimoto, T. Miyazaki, G. Mizutani, and S. Ushioda, Surf. Sci. **427-428**, 147 (1999).
[8] C. Matranga and P. Guyot-Sionnest, J. Chem. Phys. **115**, 9503 (2001).
[9] T. Kitahara, H. Tanaka, Y. Nishioka, and G. Mizutani, Phys. Rev. B **64**, 193412 (2001).
[10] R. N. Ward, P. B. Davies, and C. D. Bain, J. Phys. Chem. **97**, 7141 (1993).
[11] M. Himmelhaus, F. Eisert, M. Buck, and M. Grunze, J. Phys. Chem. B **104**, 576 (2000).
[12] A. Lagutchev, S. A. Hambir, and D. D. Dlott, J. Phys. Chem. C **111**, 13645 (2007).
[13] J. J. Wang, H. Dubost, A. Ghalgaoui, W. Q. Zheng, S. Carrez, A. Ouvrard, and B. Bourguignon, Surf. Sci. **626**, 26 (2014).
[14] A. Le Rille and A. Tadjeddine, J. Electroanal. Chem. **467**, 238 (1999).
[15] P. A. Covert and D. K. Hore, J. Phys. Chem. C **119**, 271 (2015).
[16] L. Dreesen, C. Humbert, M. Celebi, J. J. Lemaire, A. A. Mani, P. A. Thiry, and A. Peremans, Appl. Phys. B: Lasers Opt. **74**, 621 (2002).
[17] A. A. Mani, L. Dreesen, P. Hollander, C. Humbert, Y. Caudano, P. A. Thiry, and A. Peremans, Appl. Phys. Lett. **79**, 1945 (2001).
[18] C. Humbert, B. Busson, C. Six, A. Gayral, M. Gruselle, F. Villain, and A. Tadjeddine, J. Electroanal. Chem. **621**, 314 (2008).
[19] D. Elsenbeck, S. K. Das, and L. Velarde, Phys. Chem. Chem. Phys. **19**, 18519 (2017).
[20] T. A. Ishibashi and H. Onishi, Appl. Phys. Lett. **81**, 1338 (2002).
[21] M. L. Clark, B. Rudshteyn, A. M. Ge, S. A. Chabolla, C. W. Machan, B. T. Psciuk, J. Song, G. Canzi, T. Q. Lian, V. S. Batista, and C. P. Kubiak, J. Phys. Chem. C **120**, 1657 (2016).
[22] S. H. Lin and A. A. Villaeys, Phys. Rev. A **50**, 5134 (1994).
[23] B. Busson and A. Tadjeddine, J. Phys. Chem. C **113**, 21895 (2009).
[24] L. Dalstein, M. Ben Haddada, G. Barbillon, C. Humbert, A. Tadjeddine, S. Boujday, and B. Busson, J. Phys. Chem. C **119**, 17146 (2015).
[25] X. Zhuang, P. B. Miranda, D. Kim, and Y. R. Shen, Phys. Rev. B **59**, 12632 (1999).
[26] B. Busson and A. Tadjeddine, J. Phys. Chem. C **112**, 11813 (2008).
[27] R. L. Olmon, B. Slovick, T. W. Johnson, D. Shelton, S. H. Oh, G. D. Boreman, and M. B. Raschke, Phys. Rev. B **86**, 235147 (2012).
[28] M. A. Hines, J. A. Todd, and P. Guyot-Sionnest, Langmuir **11**, 493 (1995).
[29] R. Braun, B. D. Casson, C. D. Bain, E. W. M. van der Ham, Q. H. F. Vrehen, E. R. Eliel, A. M. Briggs, and P. B. Davies, J. Chem. Phys. **110**, 4634 (1999).
[30] N. Watanabe, H. Yamamoto, A. Wada, K. Domen, C. Hirose, T. Ohtake, and N. Mino, Spectrochim. Acta, Part A **50**, 1529 (1994).
[31] C. Hirose, N. Akamatsu, and K. Domen, J. Chem. Phys. **96**, 997 (1992).
[32] Z. Guo, W. Zheng, H. Hamoudi, C. Dablemont, V. A. Esaulov, and B. Bourguignon, Surf. Sci. **602**, 3551 (2008).
[33] W. Gan, B. H. Wu, Z. Zhang, Y. Guo, and H. F. Wang, J. Phys. Chem. C **111**, 8716 (2007).
[34] K. C. Jena, K. K. Hung, T. R. Schwantje, and D. K. Hore, J. Chem. Phys. **135**, 44704 (2011).
[35] D. K. Hore, D. K. Beaman, D. H. Parks, and G. L. Richmond, J. Phys. Chem. B **109**, 16846 (2005).
[36] B. Bourguignon, W. Q. Zheng, S. Carrez, A. Ouvrard, F. Fournier, and H. Dubost, Phys. Rev. B **79**, 125433 (2009).
[37] C. G. T. Feugmo, V. Liegeois, and B. Champagne, J. Phys. Chem. C **119**, 3180 (2015).
[38] T. Ishiyama, V. V. Sokolov, and A. Morita, J. Chem. Phys. **134**, 024510 (2011).
[39] E. Tyrode, C. M. Johnson, S. Baldelli, C. Leygraf, and M. W. Rutland, J. Phys. Chem. B **109**, 329 (2005).

[40]R. Lu, W. Gan, B. H. Wu, Z. Zhang, Y. Guo, and H. F. Wang, J. Phys. Chem. B **109**, 14118 (2005).
[41]H. Wu, W. K. Zhang, W. Gan, Z. F. Cui, and H. F. Wang, J. Chem. Phys. **125**, 133203 (2006).
[42]F. Vidal, A. Tadjeddine, C. Humbert, L. Dreesen, A. Peremans, P. A. Thiry, and B. Busson, J. Electroanal. Chem. **672**, 1 (2012).
[43]L. Velarde and H. F. Wang, J. Chem. Phys. **139**, 084204 (2013).
[44]M. Guerrisi, R. Rosei, and P. Winsemius, Phys. Rev. B **12**, 557 (1975).
[45]B. Busson and L. Dalstein, "Nonlinear optical response of a gold surface in the visible range: A study by two-color sum-frequency generation spectroscopy. II: Model for gold nonlinear susceptibility," J. Chem. Phys. (submitted).